Modulated light absorption and emission of a luminescent layer by phase-controlled multiple beam illumination

G. Pirruccio[1] **and Jaime Gómez Rivas**[1,2]

[1] *FOM Institute for Atomic and Molecular Physics AMOLF, c/o Philips Research Laboratories, High Tech Campus 4, 5656 AE, Eindhoven, The Netherlands*
[2] *COBRA Research Institute, Eindhoven University of Technology, P.O. Box 513, 5600 MB Eindhoven, The Netherlands*
**rivas@amolf.nl*

Abstract: We propose a multiple beam illumination scheme to control the intensity of the light emitted by a thin luminescent layer. The experiment is designed to get as close as possible to the condition of Coherent Perfect Absorption (CPA) at a wavelength at which the absorption coefficient of the luminescent layer is low, and it is realized by externally acting on the phase difference between the incident beams. We elucidate experimental limitations that prevent the achievement of CPA in these slabs. Nevertheless, we are able to demonstrate that when the two beams destructively interfere outside the luminescent layer, the incident light is more efficiently absorbed by the luminescent layer and the intensity of the emitted light is phase-modulated.

OCIS codes: (020.1670) Coherent optical effects; (080.2208) Fabrication, tolerancing; (140.3298) Laser beam combining; (290.0290) Scattering; (300.1030) Absorption; (300.2140) Emission.

References and links

1. Y. D. Chong, L. Ge, H. Cao, and A. D. Stone, "Coherent perfect absorbers: time-reversed lasers," Phys. Rev. Lett. **105**, 053901 (2010).
2. T. S. Kao, S. D. Jenkis, J. Ruostekoski, and N. I. Zheludev, "Coherent control of nanoscale light localization in metamaterial: creating and positioning isolated subwavelength energy hot spots," Phys. Rev. Lett. **106**, 085501 (2011).
3. J. Zhang, K. F. MacDonald, and N. I. Zheludev, "Controlling light-with-light without nonlinearity," Light: Sci. Appl. **1**, e18 (2012).
4. H. Noh, Y. Chong, A. D. Stone, and H. Cao, "Perfect coupling of light to surface plasmons by coherent absorption," Phys. Rev. Lett. **108**, 186805 (2012).
5. I. M. Vellekoop and A. P. Mosk, "Focusing coherent light through opaque strongly scattering media," Opt. Lett. **32**, 2309–2311 (2007).
6. B. Gjonaj, J. Aulbach, P. M. Johnson, A. P. Mosk, L. Kuipers, and A. Lagendijk, "Active spatial control of plasmonic fields," Nat. Photon. **5**, 360–363 (2011).
7. A. P. Mosk, A. Lagendijk, G. Lerosey, and M. Fink, "Controlling waves in space and time for imaging and focusing in complex media," Nat. Photon. **6**, 283–292 (2012).
8. J. Yoon, K. H. Seol, S. H. Song, and R. Magnusson, "Critical coupling in dissipative surface-plasmon resonators with multiple ports," Opt. Expr. **18**, 25702–25711 (2010).
9. J. W. Yoon, G. M. Koh, S. H. Song, and R. Magnusson, "Measurement and modeling of a complete optical absorption and scattering by coherent surface plasmon-polariton excitation using a silver thin-film grating," Phys. Rev. Lett. **109**, 257402 (2012).

#234535 Received 25 Feb 2015; revised 19 Jun 2015; accepted 23 Jun 2015; published 6 Jul 2015

10. S. Dutta-Gupta, R. Deshmukh, A. V. Gopal, O. J. F. Martin, and S. Dutta Gupta, "Coherent perfect absorption mediated anomalous reflection and refraction," Opt. Lett. **37**, 4452–4454 (2012).
11. S. Dutta-Gupta, O. J. F. Martin, S. Dutta Gupta, and G. S. Agarwal, "Controllable coherent perfect absorption in a composite film," Opt. Expr. **20**, 1330–1336 (2014).
12. K. Nireekshan Reddy and S. Dutta Gupta, "Light-controlled perfect absorption of light," Opt. Lett. **38**, 5252–5255 (2013).
13. W. Wan, Y. Chong, L. Ge, H. Noh, A. D. Stone, and H. Cao, "Time reversed lasing and interferometric control of absorption," Science **331**, 889–892 (2011).
14. A. Yariv, "Universal relations for coupling of optical power between microresonators and dielectric waveguides," Electron. Lett. **36**, 4 (2000).
15. A. Yariv, "Critical coupling and its control in optical waveguide-ring resonator systems," IEEE Photon. Technol. Lett. **14**, 4 (2000).
16. G. Blasse, and A. Bril, "Investigation of some Ce^{3+} - activated phosphors," J. Chem. Phys. **47(12)**, 5139 (1967).
17. G. Blasse, and A. Bril, "A new phosphor for flying-spot cathode-ray tubes for color television: yellow-emitting $Y_3Al_5O_{12} - Ce^{3+}$," Appl. Phys. Lett. **11(2)**, 53 (1967).
18. C. M. Wong, S. R. Rotman, and C. Warde, "Optical studies of cerium doped yttrium aluminum garnet single crystals," Appl. Phys. Lett. **44**, 1038 (1984).
19. R. Apetz and M. P. B. van Bruggen, "Transparent alumina: a light-scattering model," J. Am. Ceram. Soc. **86**[3], 480–486 (2003).
20. P. Schlotter, R. Schmidt, and J. Schneider, "Luminescence conversion of blue light emitting diodes," Appl. Phys., A Mater. Sci. Process. **64**(4), 417–418 (1997).
21. R. Mueller-Mach, G. O. Mueller, M. R. Krames, O. B. Schehin, P. J. Schmidt, H. Bechtel, C. Chen, and O. Steigelmann, "All-nitride monochromatic amber-emitting phosphor-converted light-emitting diodes," Phys. Status Solidi RRL **3**, 215–218 (2009).
22. A. Ikesue and I, Furusato, "Fabrication of polycrystalline, transparent YAG ceramics," J. Am. Ceram. Soc. **78**[1], 225–228 (1995).
23. R. Boulesteix, A, Maitre, L. Chraetien, Y. Rabinovitch, and C. Salla, "Microstructural evolution during vacuum sintering of Yttrium Aluminum garnet transparent ceramics: toward the origin of residual porosity affecting the transparency," J. Am. Ceram. Soc. **9**, 1724-1731 (2013).
24. S. Chen, L. Zhang, K. Kisslinger, and Y. Wu, "Transparent $Y_3Al_5O_{12}$: *Li, Ce* ceramics for thermal neutron detection," J. Am. Ceram. Soc. **96**[4], 1067-1069 (2013).
25. Yu. Zorenko, V. Gorbenko, I. Konstankevych, A. Voloshinovskii, G. Stryganyuk, V. Mikhailin, V. Kolobanov, and D. Spassky, "Single-crystalline films of Ce-doped YAG and LuAG phosphors: advantages over bulk crystals analogues," J. Luminescence **114(2)**, 85–94 (2005).
26. Pochi-Yeh, *Optical Waves in Layered Media* (John Wiley and Sons, 1998).
27. L. D. Landau, *Electrodynamics of Continuous Media* (Pergamon, 1984).
28. A. B. Munoz-Garcia, Z. Barandarian, and L. Seijo, "Antisite defects in Ce-doped YAG ($Y_3Al_5O_{12}$): first-principles study on structures and 4f5d transitions," J. Mater. Chem. **22**, 19888–19897 (2012).

1. Introduction

Coherent phenomena have been intensively studied in optics with the prospect of exploiting interference and resonant effects. In particular, the coherent control of light absorption has recently attracted considerable interest due to the possibility of building complex interference patters in and outside a structure, with the aim of enhancing or suppressing its optical response [1–4]. Different methods have been introduced to achieve this modulation of the response, such as wavefront shaping [5–7] and multiple beam illumination [8–12]. The essence of these works relies on the consideration that the optical absorption depends not only on the optical constants of the material, but also on the spatial distribution of the radiation. This property of the optical absorption has been theoretically studied and experimentally demonstrated by Chong and coauthors who have defined the condition for the so-called Coherent Perfect Absorption (CPA) [1, 13]. In their work they used a double side-polished silicon wafer illuminated with two collinear and counter-propagating incident beams at a wavelength at which Si is weakly absorbing to demonstrate full absorption of the incident light [13]. This work is a generalization of the concept of critical coupling [14, 15], and it is explained in terms of the optimal interplay between interference and dissipation. CPA provides the concept of total absorption by drawing the analogy with the time-reversed counterpart of lasing, in which the layer

#234535 Received 25 Feb 2015; revised 19 Jun 2015; accepted 23 Jun 2015; published 6 Jul 2015

of weakly absorbing material defines the resonant cavity. So far, research had focused only on the coherent processes related to the absorption of light, without considering or even excluding the possibility of using light converting materials [1].

In this manuscript we experimentally demonstrate that by properly setting the phase difference between two incident, counter-propagating beams of light in a luminescent layer the photoluminescence (PL) intensity can be increased and modulated. The experiment is designed to get as close as possible to the condition of CPA, i.e., the condition at which a destructive interference pattern is built outside the layer of luminescent material and the incident light is more efficiently absorbed. Since the quantum efficiency of a luminescent material can be close to unity, CPA may allow obtaining full conversion of the incident light while maintaining the thickness of the layer smaller than the absorption length. However, this point is subject to experimental limitations, which may hinder the realization of CPA, and to the structure of the energy levels of the emitting species. The presence of reabsorption may constitute a limiting factor for the efficient full conversion of the absorbed light. Therefore, reducing the layer thickness while preserving the absorption of the excitation is very relevant. To the best of our knowledge CPA in thick slabs ($h >> \lambda$, with h the layer thickness and λ the wavelength of light) has been so far demonstrated only for silicon. The imperfections in the fabrication of the slab of luminescent material may dramatically alter the response of the system, leading to a non-perfect absorption. Here, we identify the limiting factors such as surface roughness and non perfect plane-parallelity of the interfaces of the slab and we analyze their effect on the modulation of the absorption and therefore of the PL.

2. Coherent absorption in luminescent layers

Realizing CPA in luminescent materials corresponds to placing the emitters in a perfect cavity at the wavelength of the pump. Perfect means that all the incident light is trapped in the slab containing the emitters. The enhanced absorption by cavity resonances is well-known, but if the cavity and the illumination are not tuned to realize CPA, it is impossible to achieve total absorption because the scattered field (reflections at the interfaces) can not be fully cancelled. A subtle point increases the interest and novelty of systems tuned to their CPA condition: Coherent Perfect Absorbers are open systems, i.e., energy can flow efficiently inward and outward the system at the pump wavelength when the cavity is illuminated with a single beam. Only when the cavity is illuminated with two beams energy is perfectly confined inside the cavity. Typically the performance of a cavity is described by its Q-factor: a high Q indicates a low rate of energy loss (both by absorption and outcoupling) relative to the energy stored in the resonator. A high Q-factor cavity is normally realized by using very good reflecting mirrors. On the contrary, a CPA cavity does not require highly reflecting mirrors because light is trapped by the interference of the multiple incident beams.

Once the complex refractive index, $\tilde{n} = n + i\kappa$, and the thickness, h, of the luminescent slab are known, it is possible to calculate the wavelength at which the CPA condition is fulfilled. CPA is realized when the amplitudes of the scattered fields are zero. This corresponds to the condition under which the eigenvalues of the scattering matrix, S, vanishes [1]. In our experiment S is a 2x2 matrix because we use two incoming and two outgoing beams, also referred as channels [1]

$$S = \begin{pmatrix} S_{11} & S_{12} \\ S_{21} & S_{22} \end{pmatrix}. \tag{1}$$

Since the system is symmetric with respect to the plane intersecting the center of the slab $S_{12} = S_{21}$ and $S_{11} = S_{22}$. The elements S_{12} and S_{21} are the reflection coefficients, while S_{11} and S_{22} are the transmission coefficients. Since the system consists of planar and parallel interfaces, these coefficients correspond to the Fresnel reflection and transmission coefficients for a three-

#234535 Received 25 Feb 2015; revised 19 Jun 2015; accepted 23 Jun 2015; published 6 Jul 2015

layer system, r and t, respectively [26]. The eigenvalues of S are $\chi_{+,-} = S_{11} \pm S_{12} = t \pm r$. Therefore, the CPA condition can be written as

$$\chi_{+,-} = t \pm r = 0, \tag{2}$$

which in the case of the slab in air reads as

$$\frac{\left[1-\left(\frac{\tilde{n}-1}{\tilde{n}+1}\right)^2\right] e^{-ikh\tilde{n}}}{1-\left(\frac{\tilde{n}-1}{\tilde{n}+1}\right)^2 e^{-2ikh\tilde{n}}} \pm \frac{\left(\frac{\tilde{n}-1}{\tilde{n}+1}\right)\left[e^{-2ikh\tilde{n}}-1\right]}{1-\left(\frac{\tilde{n}-1}{\tilde{n}+1}\right)^2 e^{-2ikh\tilde{n}}} = 0. \tag{3}$$

This leads to the CPA condition

$$e^{ikh\tilde{n}} = \pm\frac{\tilde{n}-1}{\tilde{n}+1}, \tag{4}$$

where k is the wavevector of the incident light and the plus and the minus sign describe the symmetric and the antisymmetric mode in the slab, respectively. The symmetry refers to the electric field profile with respect to the to the plane intersecting the center of the slab. The mode relevant for our experiments will be the antisymmetric one, so in what follows we will focus on this one. If the input channel is the antisymmetric eigenvector of S, the normalized intensity of the field scattered off the slab is given by $|\chi_-|^2$. Figure 1(a) shows in logarithmic scale $|\chi_-|^2$ as a function of the real and imaginary components of the refractive index for a 100 μm-thick slab embedded in air and illuminated with a wavelength of 495.9 nm. CPA is realized for the values of $\tilde{n}$ at which the intensity of the scattered waves vanishes, thus at the minima of Fig. 1(a). To verify that for these specific combinations of n and κ of the slab the intensity of the scattered field is exactly zero, in Fig. 1(b) we plot the phase of χ_-. In correspondence with the the locations of the minima of Fig. 1(a), we find phase singularities, which indicate the complete vanishing of the scattered fields.

As reported in [1], the CPA equation has an approximated solution when $kh >> 1$, i.e., for very thick slabs compared to the incident wavelength, and in the case of very weakly absorbing materials ($\kappa << n$)

$$\begin{cases} n \approx \frac{Z\pi}{kh}, \quad Z \in \mathbb{Z} \\ \kappa \approx \frac{1}{kh}\ln\left[\frac{n+1}{n-1}\right] \end{cases} \tag{5}$$

Odd and even Z correspond to antisymmetric and symmetric CPA modes, respectively. These approximated solutions are plotted with open symbols in Figs. 1(a) and 1(b). In our experiment, described in the following sections, the imaginary component of the refractive index of the luminescent slab is on the order of $10^{-3} << n$, and its thickness is 100 μm. The wavelength used to illuminate the slab is λ_{CPA} = 495.9 nm. Thus we can use Eq. (5) to calculate in Fig. 1(c) the values of n and k at which the CPA condition is fulfilled in a ideal slab with this thickness. The inset is a zoom around the value of the complex refractive index of the luminescent slab at λ_{CPA} which is indicated by the black cross. We see that for this combination of refractive index, wavelength and thickness perfect absorption is achieved.

3. Sample preparation and characterization

The sample that we have investigated is a 100 μm-thick layer of polycrystalline lumiramic $Y_3Al_5O_{12}$ doped at 3.3% with Ce^+ ions (YAG:Ce) and polished via a chemical-mechanical procedure on both sides. YAG:Ce is an important luminescent material for lighting applications because of its superb luminescent properties, chemical durability, and thermal stability [16–18]. YAG has a cubic crystal structure which ensures no birefringence and a very high transparency [19]. YAG:Ce has an absorption peak around 460 nm while its emission spectrum spans the range between 500-750 nm. Due to its characteristic spectrum, YAG:Ce is found in

#234535 Received 25 Feb 2015; revised 19 Jun 2015; accepted 23 Jun 2015; published 6 Jul 2015

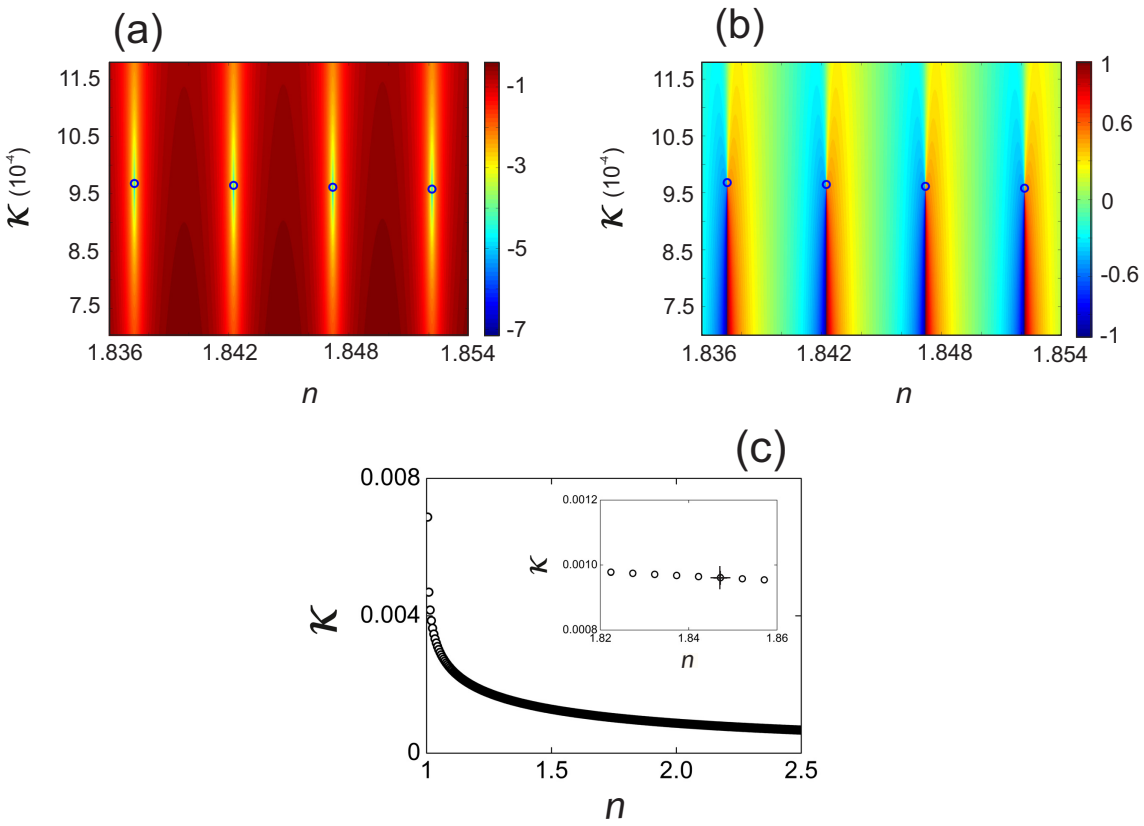

Fig. 1. (a) Calculated normalized intensity in a logarithm scale and (b) phase in units of π of the scattered field as a function of the real and imaginary component of the refractive of a 100 μm-thick slab embedded in air and illuminated antisymmetrically at normal incidence by two counter-propagating beams of wavelength of 495.9 nm. Symbols correspond to the approximated calculated solution given by Eq. (5). In (c) the approximated solution Eq. (5) for an ideal 100 μm-thick slab illuminated at the wavelength of 495.9 nm is plotted on a larger range of values of n and κ. The inset is a zoom around the value of the complex refractive index of the luminescent slab of YAG:Ce used in the experiment at this wavelength, indicated by the cross.

applications such as white light emitting diodes (LEDs) [20] and full down-conversion based devices (high-color-purity light, especially in the so-called "yellow gap" [21]). The YAG:Ce slab has been produced following the procedure described in [22–24].

A major difference between silicon, used in Ref. [13], and our emitting layer is that YAG:Ce cannot be modeled as a two-level system. YAG:Ce has a manifold electronic structure; at low temperature its emission presents two bands [25], while at room temperature the appearance of this doublet emission is not significant (see Fig. 3(b)). This complicated structure, together with the possibility of reabsorption of the emission from self-trapped excitons of the YAG host, may introduce non-linearities in the absorption and emission processes in YAG:Ce. In order to reach CPA we need to fulfil three conditions on the quality of the layer: 1) the thickness of the slab has to be uniform over the dimension of the illumination beams; 2) the surface of the sample has to be optically flat and 3) the total absence of scattering centers for the light throughout the slab. These three conditions ensure that the phase relation of the incident

#234535 Received 25 Feb 2015; revised 19 Jun 2015; accepted 23 Jun 2015; published 6 Jul 2015

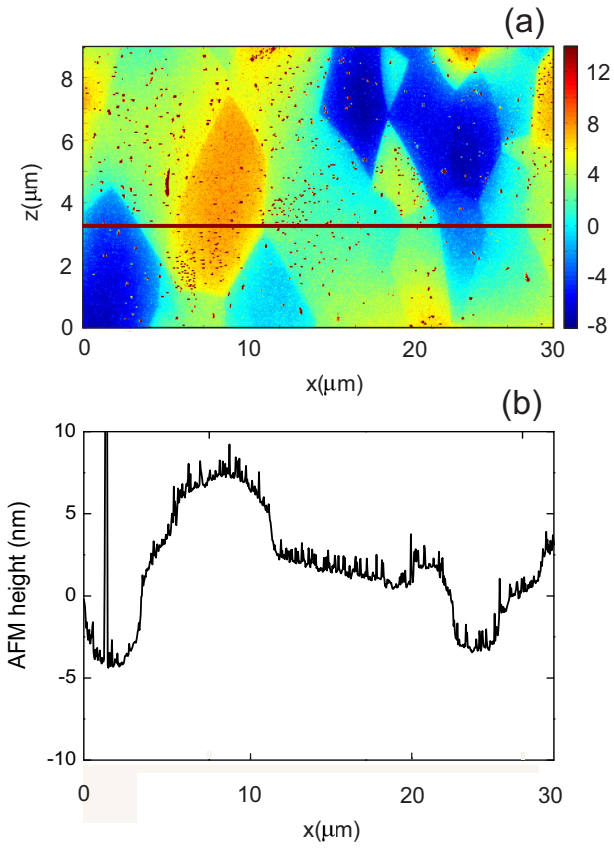

Fig. 2. (a) 2D AFM scan of the surface of the YAG:Ce slab after polishing. The colorscale indicates the relative surface height and it is in units of nanometers. (b) AFM scan along the *x*-direction at the height marked by the red line in (a).

beams imposed at the interfaces of the slab is maintained throughout the sample. To reach the desired thickness and surface quality on both interfaces of the slab, we first grinded the raw material mechanically. This is done by combining a rotating wheel with boron carbide spheres of variable size. The diameter of the spheres is varied in steps during the grinding according to the amount of material that needs to be removed. The diameter ranges from 17 μm to 6.5 μm. When approaching the desired thickness we polished the slab by using 50 nm size silica spheres in combination with KOH as a chemical etcher. The last step of the polishing was done by using KOH and aluminum oxide spheres which, being softer than the silica ones, gradually decreased in diameter during the polishing, allowing to reach an extremely smooth surface. The plane-parallelity of the surfaces of the slab was controlled by making use of several others samples of the same material that were polished simultaneously with the final sample and that avoided the off-axis motion of the polishing wheel. Nevertheless, an unavoidable small tilt of the polishing wheel could result in a slightly wedged sample. The thickness of the sample has been measured with a Heidenhain VRZ thickness gauge device. The combination of the non-perfect on-axis motion of the wheel and the precision of the VRZ is estimated to give us an accuracy on the measurement of the uniformity of the thickness of $\pm$125 nm. This uncertainty in the thickness is the main limitation that we have to take into account when interpreting the results. In Fig. 2(a) we show a 2D AFM image of the surface of the slab after the polishing

#234535 Received 25 Feb 2015; revised 19 Jun 2015; accepted 23 Jun 2015; published 6 Jul 2015

procedure. The surface roughness is on the order of 10 nm, which makes it optically flat. The height is encoded in this figure by the color scale. The regular geometrical structures visible in the figure are the polycrystals of the YAG:Ce emerging at slightly different heights because of the slightly different polishing rates along the crystallographic directions of the crystals. The dimensions of the crystals are around 5 μm. Figure 2(b) shows a cut at z=3.3 μm of the 2D AFM scan along the x direction to visualize better the surface roughness.

The complex refractive index of the material has been determined by ellipsometry. Black curves in Figs. 3(a) and 3(b) represent its real and imaginary components as a function of the wavelength. The maximum absorption is found at λ_{max} = 460 nm. The grey line in panel (b) represents the normalized emission spectrum from the YAG:Ce layer. This emission can be in general affected by its interaction with defects in the structure created during the fabrication, such as antisite defects (Y on Al site and Al on Y site), interstitials, or vacancies, especially for single crystalline (SC) thin films [28]. To avoid this situation we used bulk polycrystalline ceramic, whose garnet was made by solid state reaction of oxide raw materials. Furthermore, in our material we have created on purpose a rare earth excess, which means that a small fraction of Y is forced to Al sites. In this way it is easier to obtain fully transparent polycrystalline materials, because the solubility of Al on Y sites is much lower than the solubility of Y on Al sites. The cross section of the sample after breaking the sample into two pieces has been investigated with scanning electron microscopy. There are no inclusions, holes or imperfections

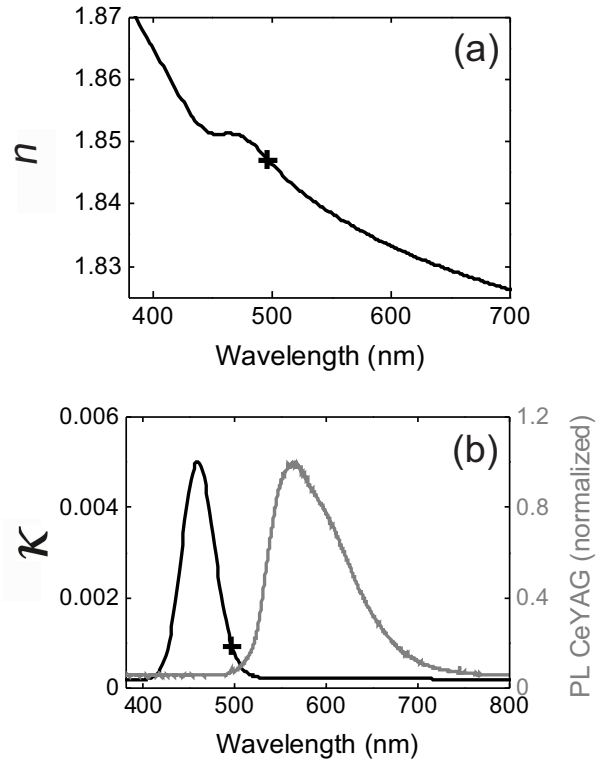

Fig. 3. Black curves represent the measured real (a) and the imaginary (b) component of the refractive index of the YAG:Ce slab as a function of the wavelength. Grey line in (b) represents the measured normalized emission spectrum from the YAG:Ce. Crosses: value of the refractive index of the YAG:Ce at 495.9 nm.

#234535 Received 25 Feb 2015; revised 19 Jun 2015; accepted 23 Jun 2015; published 6 Jul 2015

that can be attributed to the fabrication and no formation of a second phase material, which might have a different refractive index. Therefore, we can conclude that the refractive index of the material is uniform along the slab. This high quality result has been obtained by optimizing the temperature of the sintering process. The temperature determines the densification of the material. High temperature for high Ce^{+3} concentrations makes the garnet unstable, meaning that second phases, mainly $CeAlO^3$ and alumina), are generated. Keeping the temperature low is possible provided that the sintering time is sufficiently increased.

4. Experimental results

Figure 4 displays the set-up that we have used to demonstrate the coherent control on the intensity of the emitted light. A beam splitter divides a gaussian laser beam with a beam diameter (FWHM) of 2 mm, into two beams of equal intensity indicated with (1) and (2) in the figure. Beam (1) is phase delayed with respect to beam (2) through a computer-controlled piezo electrical actuator with a nanometer precise motion. The wavelength of the laser used to pump the YAG:Ce is λ_{CPA}. The two beams impinge normally on the YAG:Ce layer and get partially reflected and partially transmitted at the two interfaces. The transmitted fraction of the beam (1) interferes with the reflection of the beam (2) and the resulting intensity is monitored by a camera. Figures 4(b) and 4(c) display two images of this intensity recorded for a phase difference $\Delta\phi$ between the two beams equal to 2π and 4.5π, respectively. Because we exploit an antisym-

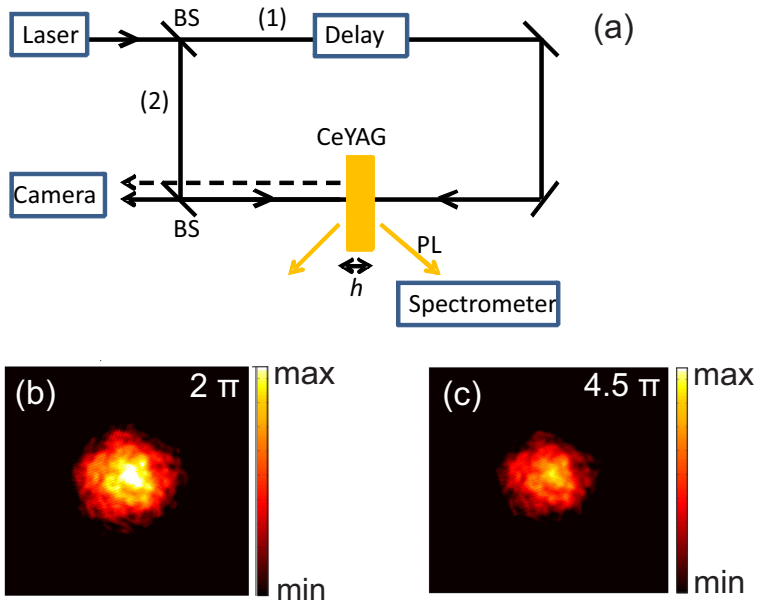

Fig. 4. (a) Schematic representation of the experimental set-up. A beam from a tunable continuous-wave Ar-Kr laser is splitted by the beam splitters (BS). The two beams (1) and (2) impinge normally to the sample, a YAG:Ce slab of thickness *h*. Beam (1) travels through a delay stage (mirror mounted on a computer-controlled piezo electrical stage) which controls the relative phase between the two beams. The scattered intensity from the left side, consisting of the interference between the backreflection of the beam (2) (continuous line) and of the transmission of beam (1) (dashed line) through the sample, is detected by a camera. The photoluminescence spectrum (PL) is measured by a spectrometer. (b) and (c) Scattered intensity recorded by the camera for $\Delta\phi = 2\pi$ and for $\Delta\phi = 4.5\pi$, respectively.

#234535 Received 25 Feb 2015; revised 19 Jun 2015; accepted 23 Jun 2015; published 6 Jul 2015

metric CPA resonance, we expect constructive interference to take place at integer numbers of π. Therefore the intensity of the signal in panel (b) is higher than the one in panel (c).

The absorbed light is converted by the YAG:Ce layer into photoluminescence emitted in a Lambertian pattern, which is detected by a spectrometer placed at a fixed angle (30°) with respect to the normal to the sample surface. The piezo electric mirror allows the control of $\Delta\phi$ [1] and the modulation of the absorption. Since the absorbed power is converted into PL by the YAG:Ce, we expect the PL and the absorptance to have the same amplitude modulation,

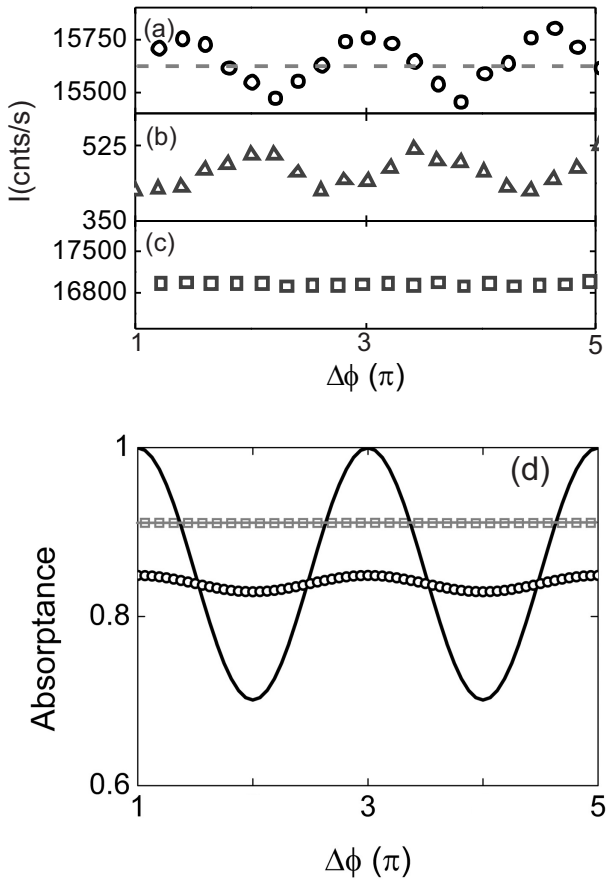

Fig. 5. Modulation of the PL from a YAG:Ce layer. (a) Measurements of the modulation of the maximum of the PL as a function of the phase difference between beam (1) and beam (2), for an incident wavelength of 495.9 nm. Grey dashed line indicates the sum of the measured maxima of the PL with the two beams separately impinging on the sample. (b) Measurements of the far field scattering in the camera. (c) As in panel (a) but for an incident wavelength of 457 nm. (d) Continuous black line: calculation of the absorptance as a function of the phase difference between beams (1) and (2) for an incident wavelength of 495.9 nm. Black circle symbols: calculated absorptance averaged over a Δh = 250 nm. Grey squares: measured absorptance for the incident wavelength 457 nm. Grey continuous line: calculated averaged absorptance over a Δh = 250 nm for the incident wavelength 457 nm.

#234535 Received 25 Feb 2015; revised 19 Jun 2015; accepted 23 Jun 2015; published 6 Jul 2015

which can be evaluated as

$$M = \frac{I(\lambda_{\mathrm{CPA}}, \Delta\phi = 2\pi m) - I(\lambda_{\mathrm{CPA}}, \Delta\phi = \pi m)}{[I(\lambda_{\mathrm{CPA}}, \Delta\phi = 2\pi m) + I(\lambda_{\mathrm{CPA}}, \Delta\phi = \pi m)]/2}, \tag{6}$$

where I is either the absorptance or the PL and m is an integer. We have measured the PL spectrum of the YAG:Ce layer for each phase difference between the two incident beams ranging from π to 5π. The black circles in Fig. 5(a) represent the maximum of the PL spectrum as a function of $\Delta\phi$. The measurement follows a cosine square function which is expected for the interference of plane wavesand only depends on the phase difference between the two incident waves. The grey dashed line in Fig. 5(a) indicates the sum of the maxima of the PL when the two beams impinge separately onto the sample. This intensity corresponds to the incoherent sum of the two beams. We reach an experimental modulation of the PL of 2.3%. We have checked the reproducibility of these results by changing the position of the illumination spot on the sample, obtaining similar modulations at all the different positions. Figure 5(b) shows the analysis of the measurements of the scattered field recorded by the CCD camera. Each point is the average intensity at the full width at half maximum of the beam spot in the camera (see Figs. 4(b) and 4(c)). This intensity is expected to be in antiphase with respect to the PL modulation, i.e., when the interference pattern outside the layer is destructive (minima in Fig. 5(b)), the energy is trapped into the layer and converted into PL (maxima in the PL modulation in Fig. 5(a)).

5. Discussion

The measured modulation of the scattered intensity and of the PL emission presented in the previous section were moderated considering that the sample thickness, refractive index, and the wavelength of the illumination were chosen to meet the CPA condition. In this section we describe the origin of this moderated modulation.

By knowing the complex refractive index of the slab and its thickness we can calculate the absorptance of an ideal slab as a function of the phase difference between the two incident waves. The phase is set at the first interface encountered by each incident wave. For each phase and for each incident wave we make use of the transfer matrix method and the superposition principle to find the values of the total electric field in the slab. The absorptance is then evaluated as the volume integral of the dissipated power in the slab [27]. The result for an ideal slab of thickness h_0 = 100 μm is plotted in Fig. 5(d) with a continuous black line as a function of the phase difference between the two beams. The absorption reaches 100% when the two waves are in antiphase, meaning that this absorption is caused by the antisymmetric CPA solution. The modulation of this absorptance is M = 35%.

The CPA condition is very sensitive to the parameters and small variations in these parameters might result in large differences between the experiment and the calculations. Experimentally, the most difficult parameter to control is the plane-parallelity of the two sample interfaces. This parallelity needs to be accurate in a nanometer scale over the full illumination area, i.e., the beam spot size of 2 mm. In Fig. 6(a) we show in a logarithmic scale the calculated normalized intensity of the scattered field, evaluated as the antisymmetric $|\chi_-|^2$. The calculation is performed as a function of the thickness of the slab and of the wavelength of illumination. As in Fig. 1(a) the regions of minimum intensity correspond to the CPA condition. This condition appears as a continuous band because λ and h appear as a ratio in the dimensionless parameter kd in the exponent of the CPA equation [Eq. (4)]. This dependence is helpful because it potentially allows tuning continuously one of the two parameters in order to compensate for a non-optimal value of the other. For instance, in the ideal case of perfect plane-parallelity and no surface roughness, it is possible to tune the system to the CPA resonance by tuning the wavelength of

#234535 Received 25 Feb 2015; revised 19 Jun 2015; accepted 23 Jun 2015; published 6 Jul 2015

the laser, as the vertical cut of $\log|\chi_-|^2$ shows in Fig. 6(b). Nevertheless, we also see that this band is very narrow both in wavelength and in thickness.

For the measurements we used as a source a continuous wave gas laser which provides an intense, stable and symmetric beam spot at the wavelength of λ_{CPA} = 495.9 nm from an atomic transition and therefore it is much sharper than the linewidth of our CPA resonance. However, due to the limitations in the fabrication, our slab is not ideal and the thickness may not be constant over the full size of the beam spot. Two factors contribute to the non-uniformity of the slab, i.e., the plane-parallelity of the two interfaces and the surface roughness. In what follows we analyze the two factors separately, meaning that we consider two scenarios: a slab with non-perfect plane-parallelity but no surface roughness and a slab with perfect plane-parallelity but with surface roughness. The first case can be modeled as a wedge, where the range of thicknesses is given by the uncertainty of the fabrication, i.e., Δh = 250 nm. The second case can be modeled with a gaussian distribution of thicknesses obtained from Fig. 2. The standard deviation of this gaussian is σ = 4.8 nm. In both cases it is possible to calculate the weighted

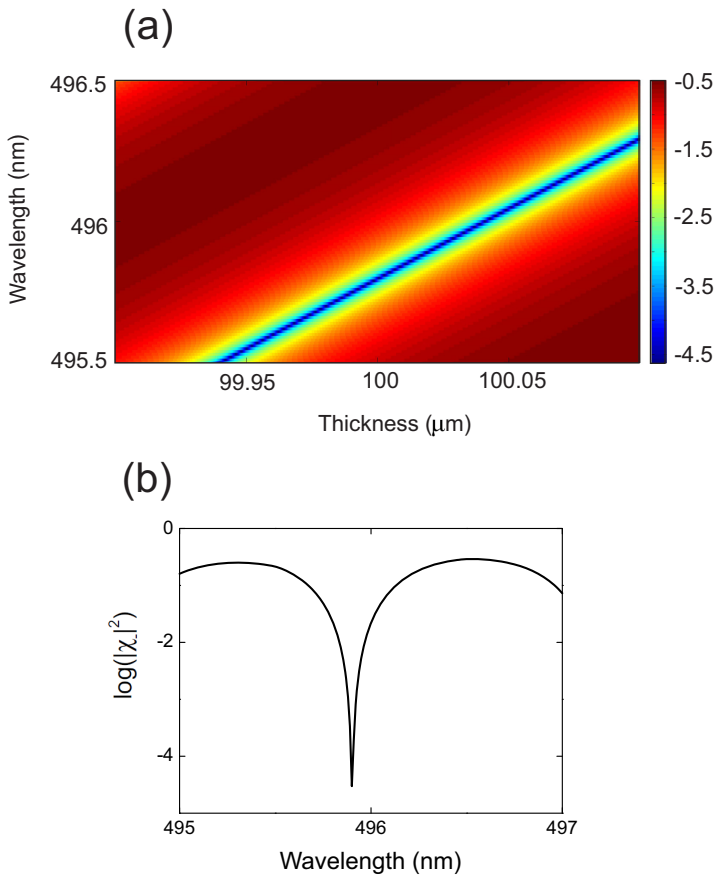

Fig. 6. (a) Calculated normalized intensity in logarithmic scale of the field scattered off a YAG:Ce slab illuminated at normal incidence by two counter-propagating beams, $\log|\chi_-|^2$, as a function of the wavelength of illumination and thickness of the slab. (b) Cut of $\log|\chi_-|^2$ for h = 100 μm.

#234535 Received 25 Feb 2015; revised 19 Jun 2015; accepted 23 Jun 2015; published 6 Jul 2015

average of the absorptance of the slab, $< A(\Delta\phi) >$, over the range of thicknesses, i.e.,

$$< A(\Delta\phi) >= \frac{\int w(h)A(h,\Delta\phi)dh}{\int w(h)dh}, \tag{7}$$

where h is the thickness at each location x of the slab. We assume the slab to be wedged only along the x-direction. The weight function $w(h)$ in the case of wedge is defined as

$$w(h) = \begin{cases} 1 & \text{for} \quad h_0 - \frac{\Delta h}{2} \leq h \leq h_0 + \frac{\Delta h}{2} \\ 0 & \text{for} \quad h < h_0 - \frac{\Delta h}{2} \quad \text{and} \quad h > h_0 + \frac{\Delta h}{2} \end{cases} \tag{8}$$

where h_0 = 100 μm. While in the case of the surface roughness

$$w(h) = e^{-\frac{(h-h_0)^2}{2\sigma^2}} \tag{9}$$

The black circles in Fig. 5(d) represent the absorptance calculated using Eq. (7) and (8), i.e., for the range of thicknesses describing the wedge, which modulation, M, is 2.2%. This strong reduction of the modulation can be understood by looking at Fig. 6(a), that shows that the scattered field is considerably suppressed for a limited range of thicknesses. On the other hand, when calculating the absorptance using Eq. (7) and (9), i.e., for the range of thicknesses representing the surface roughness, we obtain M = 34.9%, a value very close to the predicted one for an ideal slab. This is an expected result since σ is 50 times smaller than Δh, i.e., the surface roughness is a dominant effect only when $\Delta h \simeq 0$. Therefore, we conclude that the low value of the experimental modulation of the absorptance is mainly due to a non-perfect plane-parallelity of the YAG:Ce slab. To quantify the sensitivity of the modulation of the PL to the presence of a wedge in the sample we have calculated the modulation of the averaged absorptance as a function of Δh. In Fig. 7 we plot the result of this calculation. The averaged modulation is 35% when Δh = 0 and it oscillates when $\Delta h >$ 100 nm. This is because the average takes place over many dips of the scattered field (minima of $|\chi_-|^2$) appearing for values of the thickness close to the one realizing CPA [1]. Noticeably, we see that to maintain a PL modulation over 20% a $\Delta h \leq$ 70 nm is necessary. We also notice that a small tuning of the incident wavelength, which is impossible with our source, will not improve the result because of the presence of the non-perfect plane-parallelity.

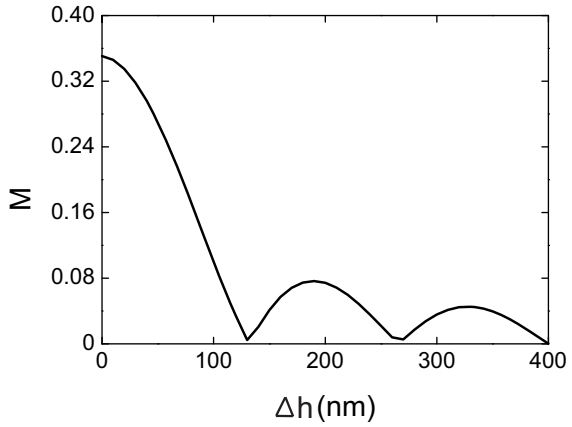

Fig. 7. Calculated averaged absorptance modulation as a function of Δh assuming no surface roughness in the YAG:Ce slab.

#234535 Received 25 Feb 2015; revised 19 Jun 2015; accepted 23 Jun 2015; published 6 Jul 2015

As a comparison we have also measured the modulation of the PL when the sample is pumped at the maximum of the absorption coefficient of the YAG:Ce, λ_{max} = 457 nm, which is usually done to obtain the maximum absorption and emission. This is shown in Fig. 5(c) with dark grey squares. In Fig. 5(d) the grey squares and the grey line represent the absorptance and the averaged absorptance for an ideal slab and for a Δh = 250 nm, respectively, for the wavelength 457 nm. The two overlap perfectly because for this wavelength the transmittance of the beams is almost 0, meaning that the transmitted light cannot modulate efficiently the reflected light. This leads to $M \simeq 0$ and an absorptance which is two times the one of the single beam.

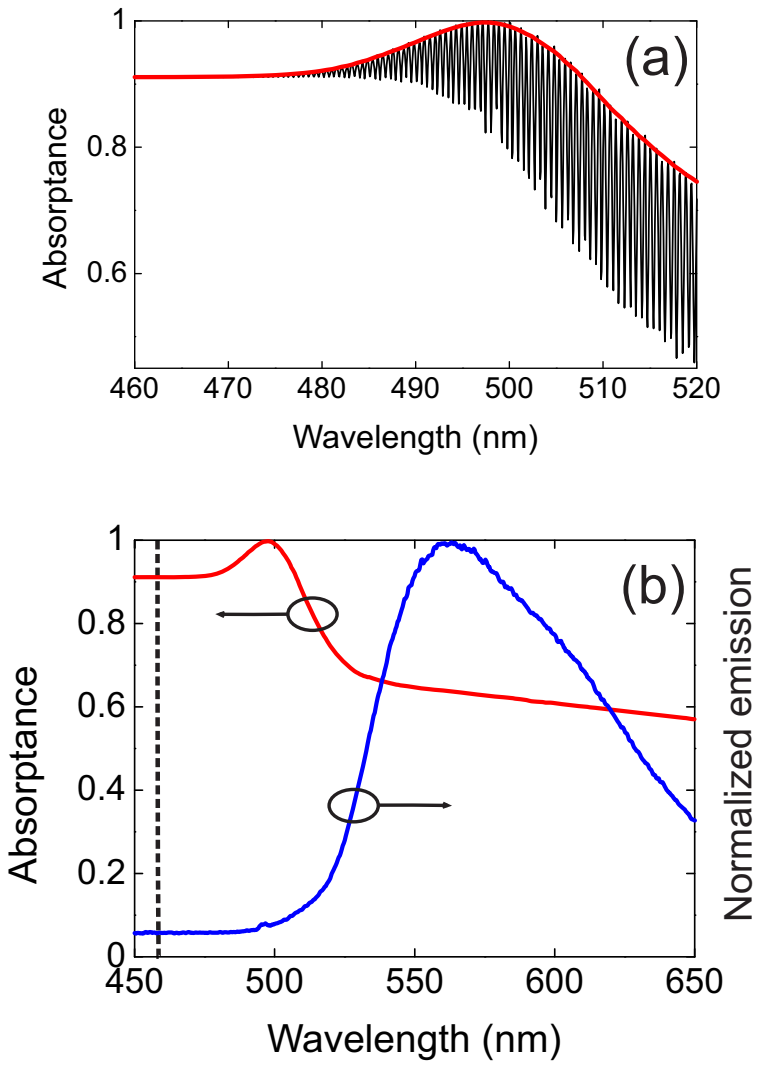

Fig. 8. (a) The black curve represents the calculated maximum absorptance at each wavelength impinging on a 100 μm-thick slab of YAG:Ce illuminated at normal incidence by two counter-proapgating and collinear beams. The red curve is the envelope of the black curve. (b) Red curve as in panel (a) on a larger range of wavelengths. The blue curve (right axis) represents the measured typical emission spectrum of YAG:Ce. The dashed line represents λ_{max}.

#234535 Received 25 Feb 2015; revised 19 Jun 2015; accepted 23 Jun 2015; published 6 Jul 2015

The strict tolerance regarding the fabrication to achieve CPA is a remarkable result, considering that CPA can be describes as the time-reversed process of lasing [1]. Lasing is a robust phenomenon which has been observed in many systems, while CPA has been so far experimentally achieved in thick silicon slabs. A reason for this might rely on the number of modes that a thick cavity filled with a gain medium sustains. Large number of modes corresponds to higher likelihood to achieve lasing in that specific cavity. The CPA experiment as realized in [13], instead, forces the all incident light to be absorbed in a single mode, increasing the sensitivity of CPA to imperfections in the fabrication.

Any down-conversion process responsible for light emission, is associated with a loss of energy determined by the characteristic Stokes' shift of the luminescent material. The Stokes' shift is defined as the difference in energy between the maximum of the absorption spectrum and the maximum of the emission spectrum. This loss is generally considered unavoidable in conversion processes. The definition of the Stokes' shift is solely related to the material, and does not take into account the role played by the geometry of the light-converting material and by the illumination conditions. Remarkably, we notice that $\lambda_{\mathrm{CPA}} > \lambda_{\mathrm{max}}$, i.e., perfect absorption is achieved at a wavelength longer than the wavelength of maximum absorption given by the optical constants of the material. This implies that the definition of the Stokes' shift needs to be modified in a perfect absorber. To illustrate the modification of the Stokes' shift, we first repeat the calculation of the absorptance as a function of the phase difference between the two beams for an ideal 100 μm-thick slab for a broad range of wavelengths. Due to the effect of the interference, each of these absorptance curves will have a maximum and a minimum. For each curve we extract the maximum value of absorptance and we plot it as a function of the wavelength in Fig. 8(a) (black curve). We see a very fast oscillation of the absorptance as a function of the wavelength, which is given by the combination of the two Fabry-Perot resonances associated with the two beams interfering in the slab. The contrast of the oscillations is reduced as the wavelength approaches λ_{max} because the transmittance of the single wave through the slab decreases due to absorption hampering the interference between the two waves. Instead, the absorptance reaches 1 at λ_{CPA}, as expected. The red curve in Fig. 8(a) is the envelope of the black curve. This envelope is plotted on a broader wavelength range in Fig. 8(b), together with the typical emission spectrum of the YAG:Ce (blue curve). By comparing the maximum of the envelope with the maximum of the emission spectrum we can conclude that the Stokes' shift can be reduced by 35% as a result of the CPA, provided that the limitations in the plane-parallelity of the layer and its surface roughness can be overcome.

6. Conclusions

We have analyzed the possibility of realizing Coherent Perfect Absorption (CPA) in a luminescent layer of weakly absorbing material relevant for solid state lighting applications. The CPA may allow for the total absorption of the incident light by the weakly absorbing layer. For luminescent materials that are not affected by reabsorption CPA establishes the upper limit for the amount of converted light that can be generated. We have highlighted the limitations that the imperfections due to the fabrication of the slab can rise and we have described the effect of those on the optical response of the system. We stress that the tolerance in the properties of the slab to achieve CPA is extremely low. This may hamper the experimental observation of CPA in systems made of materials that cannot be fabricated in an extremely controlled way. Despite of these limitations, which prevent us from fully reaching the condition for CPA, we have experimentally demonstrated the possibility of external control and modulation of the intensity of the light emitted by a layer of YAG:Ce near the condition for CPA. The result is obtained with two counter-propagating beams illuminating the sample and creating a destructive interference pattern outside the layer. The pump light is trapped in the luminescent layer where it is

#234535 Received 25 Feb 2015; revised 19 Jun 2015; accepted 23 Jun 2015; published 6 Jul 2015

eventually absorbed and converted.

Acknowledgments

This work was supported by the Netherlands Foundation Fundamenteel Onderzoek der Materie (FOM) and the Nederlandse Organisatie voor Wetenschappelijk Onderzoek (NWO), and is part of an industrial partnership program between Philips and FOM. This work is also supported by NanoNextNL, a micro and nanotechnology consortium of the Government of the Netherlands and 130 partners. The authors acknowledge G. Lozano, G. Grzela, A. Mosk and R. Maas for useful discussions, J. Boerekamp and S. Spoor for the fabrication of the sample.

#234535 Received 25 Feb 2015; revised 19 Jun 2015; accepted 23 Jun 2015; published 6 Jul 2015